

PHYSICAL REVIEW B

CONDENSED MATTER

THIRD SERIES, VOLUME 38, NUMBER 15

15 NOVEMBER 1988-II

Structural analysis of the Pt(110)-(1×2) surface using medium-energy ion scattering

P. Fenter

*Department of Physics and Laboratory for Research on the Structure of Matter, University of Pennsylvania,
Philadelphia, Pennsylvania 19104*

and Department of Physics and Astronomy, P.O. Box 849, Rutgers University, Piscataway, New Jersey 08854-0849

T. Gustafsson

Department of Physics and Astronomy, P.O. Box 849, Rutgers University, Piscataway, New Jersey 08854-0849

(Received 18 April 1988)

We have studied the geometrical structure of the Pt(110) surface using medium-energy ion scattering. We find that the structure of the reconstructed (1×2) unit cell corresponds to a missing-row model with, in contrast to previous reports, a large *contraction* of the first interlayer spacing, and a buckling of the third layer. The model, which includes deep distortions, is very similar to the one recently established for Au(110)-(1×2). In addition, we have observed the CO-induced (1×1) phase, and find that it is well described as a disordered surface.

I. INTRODUCTION

The (110) surfaces of fcc metals consist of close-packed rows along the $[1\bar{1}0]$ direction, well separated from each other in the perpendicular $[001]$ direction. This open and anisotropic character makes them likely candidates for interesting structural rearrangements. While the clean (110) surfaces of Cu,¹ Ni,² and Ag (Ref. 3) yield (1×1) LEED (low-energy electron diffraction) patterns and are therefore bulk terminated, Au(110),⁴⁻⁶ Pt(110) (Ref. 7), and Ir(110) (Ref. 8) reconstruct. The size of the unit cell is doubled along the $[001]$ direction, corresponding to a (1×2) unit cell. Of these three systems, the Au(110) surface has been most studied.⁴⁻⁶ The structure has been shown, with several techniques, to be a missing-row reconstruction with large distortions of atomic positions extending at least three layers into the bulk. At present, there exists no such consensus for the Pt(110)-(1×2) surface. The earliest structural study of Pt(110) was a high-energy ion scattering (HEIS) study,⁹ which ruled out a row-pairing model and was consistent with (but did not conclusively prove) a missing-row model. A subsequent LEED I - V study of Adams *et al.* also favored a missing-row model with a large *expansion* of the first interlayer spacing.¹⁰ Data from a later HEIS study of Jackman *et al.* were interpreted to mean that the atoms in the reconstructed phase were in bulklike positions, or at the very most displaced 5% of the interlayer spacing away from these positions.¹¹

Information about the structure may be inferred from the occurrence of adsorbate induced (1×2) to (1×1)

transitions on some of these surfaces, like the one induced by CO at room temperature on Pt(110). Using single atom diffusion data to estimate the time needed for atoms to move from step edges to fill the missing rows in this transition, Bonzel and Ferrer argued that the missing-row model was inadequate and instead suggested a sawtooth model.¹² However, a field-ion-microscopy study has found that the mobility of surface atoms above room temperature is greater than previously believed.¹³ In addition, a recent low-energy ion scattering experiment ruled out all but the missing-row model, but left open the question of the positions of the atoms within this unit cell.¹⁴ Theoretical calculations, using different methods, usually predict that the missing-row model is the most stable one,¹⁵⁻¹⁷ but with significant differences concerning the atomic locations within this model.

Considering the uncertainties that exist for this surface, and the recent success of our experimental technique, medium-energy ion scattering, to elucidate the structure of Au(110)-(1×2),⁶ we found it appropriate to investigate Pt(110)-(1×2).

The outline of this paper is as follows: In Sec. II, the experimental procedures are described. In Sec. III, the results are presented. The evidence for the basic structural model is first given, followed by a discussion of those data that allow us to determine the distortions of the atomic positions within this model. In Sec. IV, our results are discussed in relationship to earlier experimental work and theoretical predictions. Finally, some conclusions are presented. Brief accounts of this work have appeared elsewhere.¹⁸

II. EXPERIMENT

Medium-energy ion scattering (MEIS) is a quantitative surface structural technique that utilizes a 50–200-keV proton beam incident in a high-symmetry crystallographic direction on a crystal.¹⁹ A small part of the incident ion flux will be backscattered after collision with the first atom along each row of atoms in the target. Because of the coulomb repulsion between the incident ion and the atomic cores, a shadow cone is formed, which greatly reduces the probability of backscattering from deeper layers in the crystal. Due to thermal vibrations and/or distortions of the atomic positions at the surface, atoms in deeper layers will be hit by the incident beam. For our experimental parameters the hitting probabilities rapidly fall to zero. Ions that scatter off subsurface layers will freely exit the crystal, unless they are blocked from exiting by another atom in the crystal. By measuring the angular distribution of the backscattered flux, we can observe such blocking dips in the backscattered ion intensity. The angular position of a blocking dip minimum relative to the bulk crystallographic direction, as well as the absolute scattering yield, therefore contains simple and direct information about atomic structure in the near-surface region.

To get detailed information about these distortions, it is necessary to simulate the experiment for different possible surface geometries and compare to experimental data. Since the cross sections for Rutherford scattering are well known in the energy range we use,^{19,20} Monte Carlo techniques can be used²¹ and a quantitative comparison can then be made between experimental and simulated yields. The input parameters into the simulations are the atomic positions and the vibrational amplitudes of all the atoms in the crystal.

The modeling of the vibrations requires some discussion. We use an isotropic one-dimensional vibrational amplitude (U_{one}) determined from a Debye model and known bulk vibrational data ($U_{\text{one}}=0.065 \text{ \AA}$). In addition, there are two important physical effects that have to be considered: Correlated vibrations between neighboring atoms²² and the enhancement of the vibrational amplitudes at the surface.²³

The effect of correlated vibrations is to lower the hitting probability for adjacent atoms. We have included this effect by rescaling U_{one} by a correlation coefficient, c , defined as $c_{ij}=(\langle U_i U_j \rangle)^{1/2}/U_{\text{one}}$, where $\langle \rangle$ denotes a thermal average of the positions of atoms i and j . The rescaled vibrational amplitude is $U'_{\text{one}}=\sqrt{1-c} U_{\text{one}}$. The rescaling has been used successfully earlier in the analysis of other ion scattering data.²⁴ The Debye model gives a correlation coefficient that is independent of temperature above the Debye temperature (Θ_D) and as a consequence is the same for many metals (for nearest-neighboring atoms, $c_{\text{Debye}}=0.4$). Θ_D for Pt is 230 K and for Au 170 K. An analysis of the bulk phonon spectra of Au gives a correlation coefficient of $c=0.3$ (Ref. 25). We have therefore used this value for our analysis.

We have also allowed for the expected enhancement of the vibrational amplitude near the surface. We have

modeled it with a surface vibrational amplitude U_S for the first two layers, which decays exponentially to the bulk vibrational amplitude with a decay length of one atomic layer spacing ($\lambda=1.39 \text{ \AA}$). Since there is little microscopic understanding of enhanced vibrational amplitudes, U_S is treated as a fitting parameter, while U_{one} of course remains fixed.

Comparison of simulated and experimental yields is done with an R -factor ("reliability"-factor) analysis, $R=(100/N)\sum(wY_{\text{expt}}-Y_{\text{calc}})^2/(wY_{\text{expt}})^2$, where Y is the yield, w is a scaling factor, and the sum is over N data points (i.e., scattering angles).¹⁹ By scaling the experimental yields by w , we can void systematic errors in determining the atomic positions due to a small error in the yield. The R factors shown in the figures below all refer to $w=1.0$, although we found it useful to vary this parameter when searching for the optimal structure. In simulating the experiment for various geometrical parameters and surface vibrational amplitudes, a minimum R factor can be found. In this way atomic positions can, in favorable cases, be determined to within a few hundredths of an \AA .

Our ultrahigh vacuum (UHV) system, with a base pressure of less than 10^{-10} Torr, is coupled via a differentially pumped beam line to a 200 keV ion accelerator.²⁶ The backscattered protons are detected with a toroidal electrostatic energy analyzer with an angular acceptance of 20° and a resolution of $\approx 0.1^\circ$.

Since we detect only charged particles, we must determine the fraction of the backscattered particles that are charged, P^+ . In our energy regime, this quantity is dependent upon the exit energy of the ion, and is only very weakly dependent upon the exit angle or the channeling direction.²⁷ This fraction was measured using a solid-state detector, which is equipped with a pair of capacitor plates. By applying a deflection voltage to these plates, the charged particles can be eliminated. We have found P^+ to be 0.65 at 65 keV and 0.87 at 180 keV.

The backscattering cross sections deviate from the Rutherford cross section for small angle scattering due to electronic screening. We therefore use the Molière potential, which is a numerical approximation to the Thomas-Fermi potential.²⁰ For our experimental parameters, the details of the scattering potential are not important, and the Molière potential is equivalent to other realistic proposed potentials.

Experimental yields are converted to absolute scattered yields (in units of (no. of visible atoms)/[(1×1) surface unit cell]) using an Sb implanted Si wafer of a known density (0.49 atoms/\AA^2), which, in turn, was calibrated against an existing standard. The error of this normalization, and hence, of the experimentally determined yields, should be limited to systematic errors, and therefore be $< 5\%$.

Two crystals cut from the same boule were used. Both were spark cut and mechanically polished, and subsequently repeatedly sputtered and annealed (1000°C) *in situ*. Both crystals exhibited sharp and well-formed (1×2) LEED patterns with no visible streaking. Adsorption of 10 L CO at room temperature produced a (1×1) LEED pattern with increased background intensity.

[Here 1 langmuir (L) $\equiv 10^{-6}$ Torr sec.] The data from the two crystals were consistent.

III. RESULTS

A. The structural model

A top view of an fcc(110) crystal is shown in Fig. 1. The surface consists of closed-packed rows in the $[1\bar{1}0]$ direction, separated by relatively long distances in the $[001]$ direction.

A convenient scattering geometry for determining the reconstruction model is the $(1\bar{1}0)$ scattering plane (perpendicular to the $[1\bar{1}0]$ direction) shown in Fig. 2(a). Ions are incident in the $[\bar{1}\bar{1}2]$ direction and are detected in a wide angular range including the $[114]$, $[116]$, and $[118]$ bulk crystallographic directions. In this zone, there exists two independent scattering planes, one terminating in the first layer and containing the third, fifth, etc. odd-numbered layers, the other terminating in the second layer, containing even-numbered layers.

In order to discuss the expected results of our experiments, it is useful to remember that the vibrational amplitude U_{one} is equal to 0.065 \AA , while the shadow cone radius for 65-keV protons on Pt(110) with incidence direction $[\bar{1}\bar{1}2]$ is 0.57 \AA . This means that the beam will, to a first approximation, only see 1 atom/row (assuming bulklike positions). Consequently, for an ideal (1×1) terminated surface, the data from the $(1\bar{1}0)$ plane would be quite flat with a yield of > 2 atoms/ (1×1) unit cell. If vibrations allow deeper layers to be probed, the yield will increase, and blocking dips should be observable around the $[114]$, $[116]$, and $[118]$ directions. The size of the blocking dips should decrease smoothly as higher index directions are approached. The data in Fig. 2(b) are very different. The scattering yield near the $[114]$ and $[118]$ blocking directions drops significantly below 2 atoms/unit cell. This is only possible if vacancies exist on the surface, allowing the incident beam to penetrate, but preventing the backscattered flux from exiting at these angles. In addition, the $[116]$ blocking dip is largely absent, implying that the vacancies are ordered on the sur-

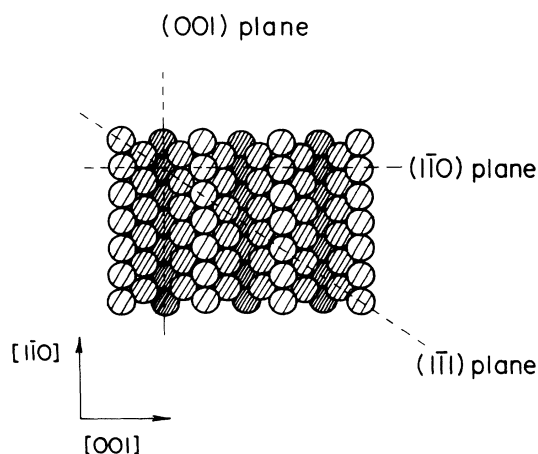


FIG. 1. A top view of the Pt(110) surface. The dashed lines indicate the scattering planes used in this study.

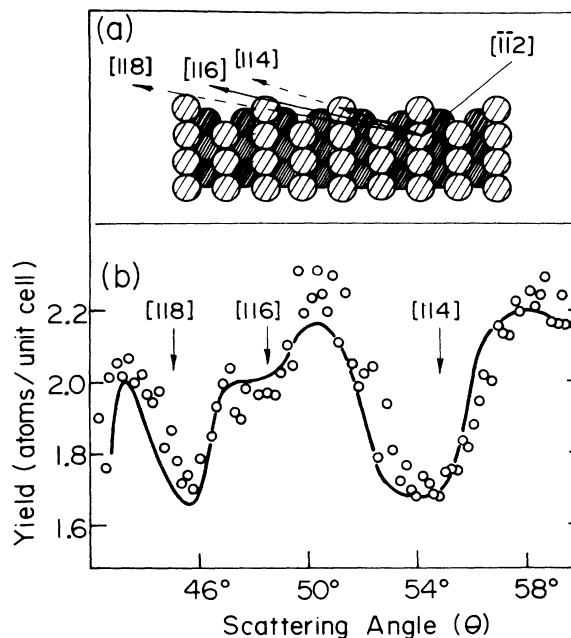


FIG. 2. (a) A side view of the $(1\bar{1}0)$ scattering plane for the missing-row model. The incident direction and three blocking directions are shown. Dashed lines indicate ion paths that are blocked. Note that there are two independent scattering planes. (b) The experimental scattered yield (open circles) as a function of scattering angle for 65-keV protons incident along the $[\bar{1}\bar{1}2]$ direction. The $[114]$, $[116]$, and $[118]$ blocking direction are indicated. A simulation for the missing-row model is shown as a solid line.

face. If these vacancies are placed at every other first-layer site [see Fig. 2(a)] the ions will be free to exit along $[116]$ but not along $[114]$ and $[118]$. The observed pattern is then a signature of a missing-row model. A Monte Carlo simulation for a missing-row model shows [Fig. 2(b)] quite good agreement with the data.

The sawtooth model was proposed to explain the rapid (1×2) -to- (1×1) phase transition upon adsorption of CO.¹² This model [shown in Fig. 3(a)] is similar to the missing-row model, but includes vacancies in *both* independent $(1\bar{1}0)$ planes. The phase transition will then require only short atomic movements. This model has the additional attractive feature that large close-packed (111) facets are created. The price one pays for this is the sharp sawtooth shape, which will be energetically costly. Theoretical calculations show indeed that this model corresponds to a very high surface energy, compared to other reconstruction models.^{15,17} Since there are twice as many vacancies in the sawtooth model as in the missing-row model, twice as many ions are scattered from the deeper layers in the crystal. Consequently, the $[114]$ and $[118]$ blocking dips would be roughly twice as deep, while the $[116]$ blocking dip should remain largely absent. Indeed, a simulation of such a structure shows these features [Fig. 3(b)], and the agreement between the simulation and experiment is significantly worse than for the missing-row model.

In order to address the nature of the (1×2) -to- (1×1)

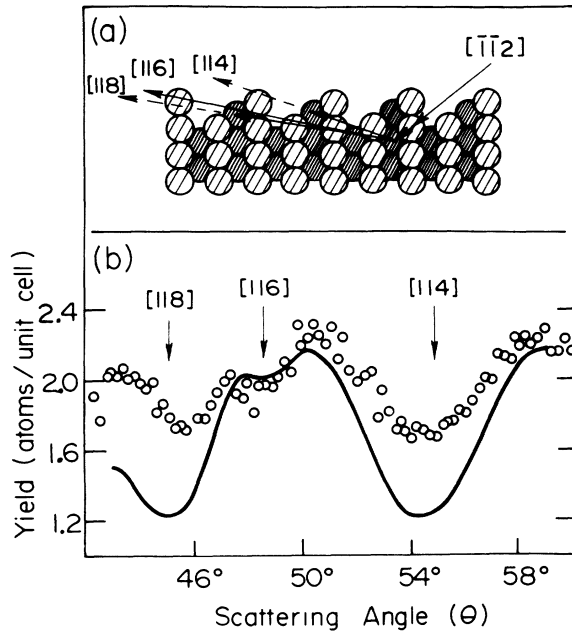


FIG. 3. (a) A side view of the $(\bar{1}\bar{1}0)$ scattering plane for the sawtooth model. Note that vacancies are present in both independent scattering planes. (b) The experimental yield (open circles) for 65-keV protons and a simulation for the sawtooth model (solid lines) as a function of the scattering angle.

phase transition, we have also observed the (1×1) phase in this scattering plane (see Fig. 4) after adsorbing 10 L of CO at room temperature. As described above, for a uniform nonreconstructed surface, the experimental yield would be greater than 2 atoms/unit cell. Again, we find that the yield drops significantly below this value near the [114] and [116] directions, implying that vacancies *still* exist in the (1×1) phase. Since we observe the [116] blocking dip (which is absent for the reconstructed surface), the correlation among the vacancies must have been reduced, implying that this structure corresponds to a disordered half monolayer of atoms sitting at lattice sites, over a nonreconstructed surface. This is supported

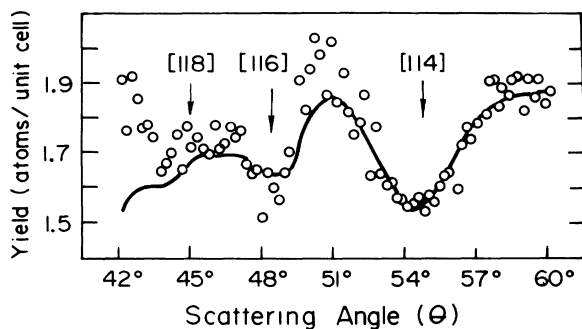


FIG. 4. Experimental yield as a function of the scattering angle for 65-keV protons incident along $[\bar{1}\bar{1}\bar{2}]$ [see Fig. 2(a)], for the CO-induced (1×1) phase. A simulation is shown (solid line) for a half monolayer of atoms randomly placed at surface lattice sites. The [114], [116], and [118] blocking directions are indicated.

by the observation of no superstructure and a higher background intensity in LEED. That we find the CO-induced phase to be disordered is consistent with the field-ion-microscopy study which found that surface atoms are mobile above room temperature.¹³ This interpretation is confirmed by a simulation of this structure (Fig. 4). The disordered half monolayer allows the beam to see the second layer, and since the overlayer is disordered these ions will be randomly blocked from exiting alone [114], [116], and [118]. The yield is accurately described near each of these directions, even near [118] where the blocking dip has been obscured by the disorder. We consider the agreement in Fig. 4 to be quite convincing, as no attempt was made to optimize the structural parameters.

The simulations in this scattering plane require a perfect correlation of vacancies across many unit cells. Since defects affect the scattered yield, they would introduce systematic errors into our analysis. We will therefore not further use these data in the more detailed structural analysis below. The simulation shown in Figs. 2–4 have all used the structural parameters as determined below.

B. Distortions

To determine the distortions of the atomic positions that accompany the missing-row reconstruction, it is convenient to use the $(\bar{1}\bar{1}1)$ scattering plane [Fig. 5(a)] as a starting point. The beam is incident along $[\bar{1}01]$ and detected near [011]. This plane allows for a simple analysis because there is only one scattering plane. The vacancies allow the beam to see every other second-layer atom, resulting in a deep blocking dip and a high sensi-

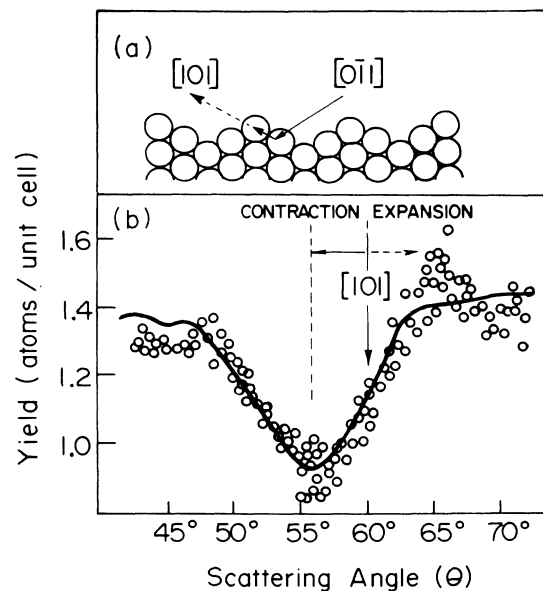


FIG. 5. (a) A side view of the $(\bar{1}\bar{1}1)$ scattering plane. (b) The experimental yield (open circles) for 65-keV protons incident along $[\bar{1}01]$ as a function of angle. Note that the blocking minimum is shifted with respect to the bulk [011] crystallographic direction. A simulation of our best structure (solid line) is shown.

tivity to the distortion of the spacing between the first and second layer. A distortion appears as a shift of the blocking dip away from the bulk blocking direction 60° . An inspection of the data shows a marked shift ($\approx 4^\circ$) to smaller scattering angles, denoting a large contraction of the first-interlayer spacing. This shift is very large by the standards of MEIS, and is similar to the one observed on Au(110).⁶ If one naively assumes that the position of the blocking dip minimum corresponds to the bond angle between the first- and second-layer atoms, the resulting contraction of the first-to-second layer spacing (Δd_{12}) is roughly 15%. As we will see below, the Monte Carlo analysis gives a value surprisingly close to this rough estimate.

Roughly speaking, there are three atoms that may be visible to the beam in this geometry [Fig. 5(a)]: The top-layer atom and two second-layer atoms (one fully visible to the beam, the other shadowed by the first-layer atom). A 15% contraction of d_{12} corresponds to a vertical displacement of 0.22 \AA , or a displacement of 0.19 \AA perpendicular to the ion beam. The top-layer atom has then moved enough so that the second-layer atom it partially shadows has a significant probability of moving out of the shadow cone ($R_c = 0.44 \text{ \AA}$) and becoming visible to the beam. These two atoms are visible to the detector at all scattering angles, while the other second-layer atom is blocked in double alignment. A simulation shows that the hitting probability for the partially shadowed atom is ≈ 0.6 which would result in a single alignment yield of $\approx (1 + 0.6 + 1)/2 = 1.3$ atoms/(1×1) unit cell, and a double alignment yield of $\approx (1 + 0.6 + 0)/2 = 0.8$ atoms/unit cell. Experimentally, the single alignment yield is 1.3 atoms/unit cell, while in double alignment we obtain 0.9 atoms/unit cell. The small differences between our estimates and the data are due to the simplicity of this analysis as well as other distortions which will be discussed below.

To determine Δd_{12} with accuracy, it is necessary to compare simulations of many trial structures with the experimental data. The two most sensitive parameters in this scattering plane are Δd_{12} and the enhanced surface vibrational amplitude, U_S . Both parameters affect the yield, while Δd_{12} has a greater effect than U_S upon the position of the surface blocking minimum. A plot of R factors versus these two parameters (Fig. 6) shows a clear

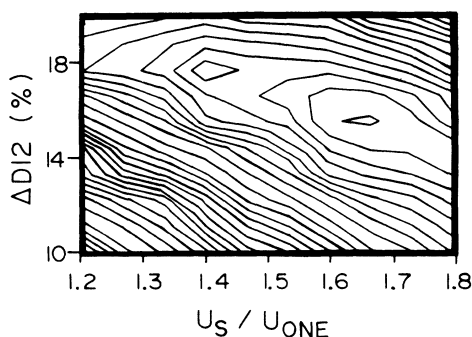


FIG. 6. An R -factor contour map, for the data shown in Fig. 5(b), as a function of the change in the first-to-second layer spacing, $\Delta d_{12}(\%)$, and the surface vibrational amplitude, U_S .

minimum for $\Delta d_{12} = -16\%$, and $U_S = 1.6U_{\text{one}}$. This corresponds to a large contraction of the first-interlayer spacing and a surface Debye temperature $\Theta_D \approx 140 \text{ K}$, in very reasonable agreement with an early LEED determination of 107 K (Ref. 28). A simulation of our best structure which includes Δd_{12} , U_S (and other parameters to be discussed) is shown in Fig. 5(b). The agreement is quite good over the whole angular range.

Two other potentially important distortions (allowed by the symmetry of the reconstructed surface) are pairing in the second layer (P_2) and buckling in the third layer (B_3). To determine these distortions, the (001) scattering plane is useful [Fig. 7(a)]. In this scattering plane, the ions are incident along $[0\bar{1}0]$, scatter along the close-packed rows, and are detected near $[100]$. For an unreconstructed surface, there would be two inequivalent scattering planes, terminating in the first and second layers, respectively. The missing-row reconstruction adds a third inequivalent plane, terminating in the third layer. In this scattering direction, we will therefore sample a superposition of the distortions in these three planes, with appropriate weighting factors. Since no vacancies are expected in any of these planes, we have used higher-energy protons (180 keV) in order to probe the second layer of atoms in each plane. If the only distortion were the inward movement of the first layer established in Fig. 5(b), we would expect an angular shift away from the bulk direction. This shift will be reduced (due to the weighting factors) compared to the $(1\bar{1}1)$ plane, but should still be easily observable. Upon inspecting the data, it is evident that there is little or no shift in the surface blocking

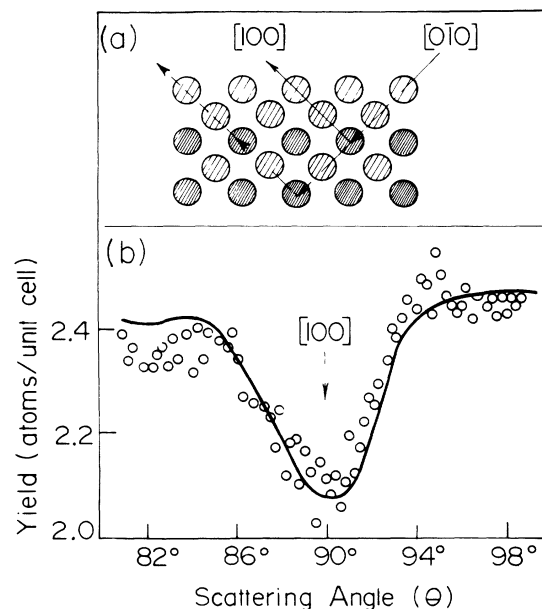


FIG. 7. (a) A side view of the (001) scattering plane. In this scattering plane, there are three inequivalent planes, and ions are shown scattering off the plane terminated by the third- and fifth-layer atoms. (b) The experimental yield (open circles) for 180-keV protons incident along $[0\bar{1}0]$ as a function of scattering angle. A simulation for our best structure (solid line) is shown. The bulk crystallographic direction is at 90° .

dip away from the bulk direction at 90° . Consequently, there must exist compensating distortions in deeper layers. One way of accomplishing this is to move the third-layer atoms (directly below the remaining top-layer atoms) towards the bulk. This reduces the change in d_{13} without affecting d_{12} . In addition, if the separation between the third and fifth layers in the plane terminated by the third layer increases, the blocking dip will be further shifted back towards the bulk value. This constitutes a *buckling* of the third layer, shown in Fig. 8.

By performing Monte Carlo simulations, these distortions can be accurately determined. Using the value of $\Delta d_{12} = -16\%$ that we determined above, we show in Fig. 9(a) an R -factor plot as a function of the pairing in the second layer, P_2 (see Fig. 8), and the vibrational amplitude, U_S . In this scattering plane, the direction of the pairing is perpendicular to the scattering plane, and the yield is therefore strongly dependent on the pairing. The results of this analysis are clearly symmetrical around $P_2 = 0 \text{ \AA}$ and favors $U_S = 1.3U_{\text{one}}$. In Fig. 9(b), we continue by plotting the R factors as a function of the buckling of the third layer, B_3 , and the change in the second-to-third layer separation, Δd_{23} . Again, a distinct minimum is found, here for a (peak-to-peak) buckling B_3 of 0.10 \AA and $\Delta d_{23} = +4\%$. A full set of these comparisons has been made resulting in a consistent picture between the two scattering planes. We find $\Delta d_{12} = -16\%$, an expansion of the second-to-third layer spacing, $\Delta d_{23} = +4\%$, a peak-to-peak buckling $B_3 = 0.10 \text{ \AA}$, and no evidence for pairing ($P_2 = 0$). A simulation for this best structure in the (001) plane is shown in Fig. 7(b), and the agreement is very good over the whole angular range.

An apparent inconsistency in the modeling has been the use of different surface vibrational amplitudes in the two scattering planes [$U_S = 1.6U_{\text{one}}$ in $(1\bar{1}1)$ and $U_S = 1.3U_{\text{one}}$ in (001)]. We have used a single correlation coefficient ($c = 0.3$) throughout our analysis. This value is appropriate for the $(1\bar{1}1)$ plane, where the distance between atoms (in the direction of the incident beam) is comparatively short. A lower correlation coefficient should be used in the (001) plane, producing a slightly larger *effective* vibration amplitude. This would require a *smaller* enhancement of the vibrational amplitude in this plane, slightly increasing the discrepancy between the scattering planes.

Another possible explanation might lie in the fact that we have used an isotropic vibrational amplitude throughout this study. Both early LEED studies²⁸ and

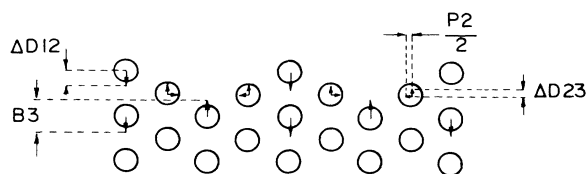


FIG. 8. A schematic picture of the distortions of atomic positions in the near-surface layers for Pt(110)-(1×2). These distortions are described in the text.

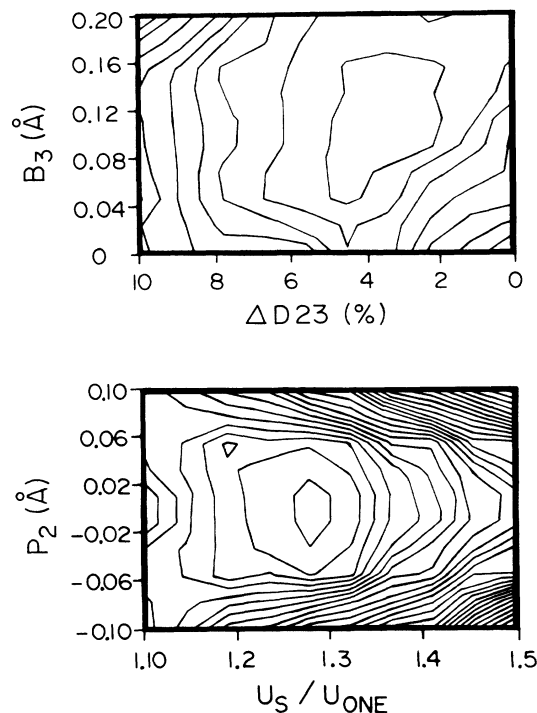


FIG. 9. R -factor contour maps for the data in Fig. 7(b) (a) as a function of the peak-to-peak third-layer buckling, B_3 , and the change in the second-to-third layer spacing, Δd_{23} , and (b) as a function of second-layer pairing, P_2 , and the surface vibrational amplitude U_S .

some simple models of surface vibrations^{29,30} have predicted large anisotropies in surface vibrational amplitudes. When we include this effect in our simulations over a restricted range of anisotropy parameters, we do not see a significant change in the minimum R factor, and the inconsistency between scattering planes remains. We have not done an exhaustive search through a full range of these parameters because MEIS is not sensitive to the detailed nature of the vibrations, and such a modeling may therefore only mask any systematic errors. However, an independent knowledge of the vibrational properties of a surface would be very desirable as it would eliminate all nonstructural parameters from an analysis of a MEIS experiment. Detailed calculations of surface phonon spectra have appeared in the literature, and anisotropic Debye temperatures for each atom could presumably be obtained from these without too much effort.^{31,32}

One potential systematic error in these comparisons between the simulated and experimentally determined blocking dip is a possible inaccuracy of the experimentally determined yields. This would tend to affect the magnitude of some of the distortions as distortions tend to raise the scattered yield. So far in our R -factor analysis, we have assumed that our experimentally determined yields were correct, which corresponds to fixing w in the above expression for the R factor to the value 1. By allowing w to vary a few percent, we allow for the possibility that the measured yields may be slightly in error. We have found using the scaled R factors that the discrepancy in the vibrational amplitude between different scatter-

ing planes can be eliminated if we assume an error in the absolute yield of $\approx 5\%$, which is the limit of our experimental uncertainty. For the purely structural parameters, the difference between the two types of analysis is small, and is included in the uncertainties.

In comparing to other determinations of the surface Debye temperature, the result of the $(\bar{1}\bar{1}1)$ scattering plane is the most relevant ($\Theta_D \approx 140$ K). In this plane, the beam is the most surface sensitive, and therefore the Debye temperature is least sensitive to the details of the vibrational model. The uncertainty in the Debye temperature can be estimated by the discrepancy between the two scattering planes, which gives ± 30 K.

IV. DISCUSSION

Previous experimentally derived structural parameters for the Pt(110) surface are inconsistent with the present results. A recent HEIS study reports no distortions in the near-surface layers (within an accuracy of $\pm 5\%$ of the interlayer spacing).¹¹ While those conclusions are incompatible with our results above, the data are in fact quite consistent. In that study, the dependence of the total backscattered flux on small variations of the incidence angle around a channeling direction was measured. Data were reported in two different scattering geometries. The first, with the beam normally incident upon the crystal, is primarily sensitive to distortions parallel to the surface. The fact that little evidence for distortion was observed here is fully consistent with our results, which show no evidence for lateral rearrangements. In the second scattering geometry, the beam was incident along $[0\bar{1}0]$, equivalent to the (001) scattering plane discussed above (see Fig. 7). Our data in this geometry were quite undramatic and symmetric. The distortions of d_{13} , d_{24} , and d_{35} , which are probed in this geometry, are indeed all less than 5%. It was the data from the $(\bar{1}\bar{1}1)$ plane (Fig. 5) that conclusively showed that large distortions do exist in this structure and this in turn led us to interpret the data in the (001) plane [Fig. 7(b)] as evidence for other large distortions in opposite directions.

The LEED I - V study of Adams *et al.* obtained the smallest R factor for a very substantial expansion.¹⁰ However, there was also a local minimum at a large contraction, consistent with the present study. Only distortions of the first and second layer were considered, and it is very reasonable to assume that if the third-layer buckling were also included, an improvement of the R factor would be obtained, as was the case for Au(110).⁵

Both of these studies point out a marked advantage MEIS has over other surface structure techniques. There can be, in simple cases, clear and straightforward evidence for some of the more important structural parameters. By a careful choice of scattering geometries, each of

these parameters can then be isolated.

Theoretical predictions of the structure of Pt(110) have been performed using both a parametrized linear combination of atomic orbitals (LCAO) approach¹⁵ and the embedded-atom method (EAM).^{16,17} These studies both predict that the missing-row model is the most stable one. The LCAO calculation predicts a first-layer contraction of 10% and a second-layer expansion of 2%. Both of these numbers are smaller than the measured values. The EAM predicts a large contraction of d_{12} (18%) and a buckling in the third layer of 0.11 Å, in excellent agreement with the present study. It was also predicted that the second-to-third layer spacing should be contracted by 5%, where we measure an expansion of the same magnitude.

In comparing with Au(110) we find Au has a slightly larger contraction of d_{12} , and an equal expansion of d_{23} (within the error limits). In addition, no significant second-layer pairing was found in either study. The most significant difference is that Au(110) has a third-layer buckling which is twice the magnitude as that found for Pt. In the case of Au(110) there is agreement among a wide variety of experiments, including MEIS (Ref. 6) and LEED.⁵

V. CONCLUSIONS

We have used MEIS to study the geometric structure of Pt(110). The data shows direct evidence that the crystal reconstructs to a missing-row reconstruction, and experiences large distortions of the interlayer spacing. We have found a contraction of the first-layer separation $\Delta d_{12} = (-16 \pm 3)\%$, a peak-to-peak buckling in the third layer of $B_3 = 0.10 \pm 0.04$ Å, an expansion in the second-to-third layer distance $\Delta d_{23} = (+4 \pm 3)\%$, and little or no pairing in the second layer ($P_2 < 0.04$ Å), as well as a 60% enhancement of the vibrational amplitude at the surface corresponding to a surface Debye temperature of 140 K. These structural parameters compare well with recent theoretical predictions. We have also observed the CO-induced (1×1) phase and find that it is well described as a disordered surface phase.

ACKNOWLEDGMENTS

We would like to thank Dr. K. Liang for supplying the crystals, and Dr. M. Copel for many valuable discussions. This research was supported by National Science Foundation (NSF) Grant No. DMR-87-03897. Use of the Central Facilities at the Laboratory for Research on the Structure of Matter at the University of Pennsylvania, supported by NSF Grant No. DMR-85-19059, is gratefully acknowledged.

¹M. Copel, T. Gustafsson, W. R. Graham, and S. M. Yalisove, Phys. Rev. B **33**, 8110 (1986).

²S. M. Yalisove, W. R. Graham, E. D. Adams, M. Copel, and T. Gustafsson, Surf. Sci. **171**, 400 (1986).

³E. Hollub-Krappe, K. Horn, J. W. M. Frenken, R. L. Krans, and J. F. van der Veen, Surf. Sci. **188**, 335 (1987).

⁴G. Binnig, H. Rohrer, Ch. Gerber, and E. Weibel, Surf. Sci. **131**, L379 (1983).

⁵W. Moritz and D. Wolf, Surf. Sci. **163**, L655 (1985).

⁶M. Copel and T. Gustafsson, Phys. Rev. Lett. **57**, 723 (1986).

⁷D. W. Blakely and G. A. Somorjai, Surf. Sci. **65**, 141 (1977).

⁸K. Christmann and G. Ertl, Z. Naturforsch. **28a**, 1144 (1973).

- ⁹E. Bøgh and I. Stensgaard, in *Proceedings of the Seventh International Vacuum Congress and the Third International Conference on Solid Surfaces, Vienna, 1977*, edited by R. Dobrozemsky, F. Rüdener, F. P. Viehböck, and A. Breth (Berger, Vienna, 1977), p. A-2757.
- ¹⁰D. L. Adams, H. B. Nielsen, M. A. van Hove, and A. Ignatiev, *Surf. Sci.* **104**, 47 (1981).
- ¹¹T. E. Jackman, J. A. Davies, D. P. Jackson, W. N. Unertl, and P. R. Norton, *Surf. Sci.* **120**, 389 (1982).
- ¹²H. P. Bonzel and S. Ferrer, *Surf. Sci.* **118**, L263 (1982).
- ¹³G. L. Kellogg, *Phys. Rev. Lett.* **55**, 2168 (1985).
- ¹⁴H. Niehus, *Surf. Sci.* **145**, 407 (1984).
- ¹⁵H.-J. Brocksch and K. H. Bennemann, *Surf. Sci.* **161**, 321 (1985).
- ¹⁶S. M. Foiles, *Surf. Sci.* **191**, L779 (1987).
- ¹⁷Murray S. Daw, *Surf. Sci.* **166**, L161 (1986).
- ¹⁸P. Fenter and T. Gustafsson, *Bull. Amer. Phys. Soc.* **32**, 772 (1987); T. Gustafsson, M. Copel, and P. Fenter, in *The Structure of Surfaces II*, edited by J. F. van der Veen and M. A. Van Hove (Springer, Berlin, 1988), p. 110.
- ¹⁹J. F. van der Veen, *Surf. Sci. Rep.* **5**, 199 (1985).
- ²⁰G. Molière, *Z. Naturforsch.* **2a**, 133 (1947).
- ²¹I. Stensgaard, L. C. Feldman, and P. J. Silverman, *Surf. Sci.* **77**, 513 (1978).
- ²²D. P. Jackson, B. M. Powell, and G. Dolling, *Phys. Lett.* **51A**, 87 (1975).
- ²³Joost W. M. Frenken, R. G. Smeenk, and J. F. van der Veen, *Surf. Sci.* **135**, 147 (1983).
- ²⁴D. P. Jackson, T. E. Jackman, J. A. Davies, W. A. Unertl, and P. D. Norton, *Surf. Sci.* **126**, 226 (1983).
- ²⁵S. P. Withrow, J. H. Barrett, and R. J. Culbertson, *Surf. Sci.* **161**, 584 (1985).
- ²⁶W. R. Graham, S. M. Yalisove, E. D. Adams, T. Gustafsson, M. Copel, and E. Törnqvist, *Nucl. Instrum. Methods B* **16**, 383 (1986).
- ²⁷R. Haight, L. C. Feldman, T. M. Buck, and W. M. Gibson, *Nucl. Instrum. Methods B* **2**, 501 (1984).
- ²⁸H. B. Lyon and G. A. Somorjai, *J. Chem. Phys.* **44**, 3707 (1966).
- ²⁹R. E. Allen and F. W. de Wette, *Phys. Rev.* **188**, 1320 (1969).
- ³⁰D. P. Jackson, *Surf. Sci.* **43**, 431 (1974).
- ³¹A. G. Eguiluz, A. A. Maradudin, and R. F. Wallis, *Phys. Rev. Lett.* **60**, 309 (1988).
- ³²K. M. Ho and K. P. Bohnen, *Phys. Rev. Lett.* **56**, 934 (1986).